Correction of Sampling Errors in Ocean Surface Cross-Sectional Estimates from Nadir-Looking Weather Radar

I. J. CAYLOR* AND G. M. HEYMSFIELD

Mesoscale Atmospheric Processes Branch, Laboratory for Atmospheres, NASA/Goddard Space Flight Center, Greenbelt, Maryland

R. MENEGHINI

Microwave Sensors Branch, Laboratory for Hydrospheric Processes, NASA/Goddard Space Flight Center, Greenbelt, Maryland

L. S. MILLER

Department of Physics and Astronomy, Clemson University, Clemson, South Carolina

4 April 1996 and 25 July 1996

ABSTRACT

The return from the ocean surface has a number of uses for airborne meteorological radar. The normalized surface cross section has been used for radar system calibration, estimation of surface winds, and in algorithms for estimating the path-integrated attenuation in rain. However, meteorological radars are normally optimized for observation of distributed targets that fill the resolution volume, and so a point target such as the surface can be poorly sampled, particularly at near-nadir look angles. Sampling the nadir surface return at an insufficient rate results in a negative bias of the estimated cross section. This error is found to be as large as 4 dB using observations from a high-altitude airborne radar. An algorithm for mitigating the error is developed that is based upon the shape of the surface echo and uses the returned signal at the three range gates nearest the peak surface echo.

1. Introduction

Microwave remote sensing of the ocean surface is a well-established field of research, and the design of instruments such as scatterometers and radar altimeters has been optimized to provide accurate measurements of the backscattered signal. During the last decade, airborne radar techniques have been developed in the meteorological community that require estimation of the normalized surface cross section (σ^o). These techniques involve using the observed cross section as a means of validating radar calibration (Durden et al. 1994) and estimating the magnitude and direction of the surface winds (Atlas and Matejka 1985; Hildebrand 1994). Airborne radars typically operate at attenuating wavelengths, and so algorithms have been developed to correct rainfall estimates for attenuation. One such algorithm, the surface reference method, involves comparing observations of the surface cross section in a cloud-free region to the cross section under regions of rain (Meneghini et al. 1983; Meneghini and Nakamura 1990; Iguchi and Meneghini 1994). However, meteorological radar systems normally are not designed for observations of point targets, and as a result, a significant error may arise in the estimate of the surface cross section for a near-nadir viewing geometry (Kozu et al. 1995).

While weather radar is designed for targets uniformly distributed in the pulse volume, the surface is a point, or impulse, target. The surface echo at nadir incidence is a narrow feature that will appear only in two or three range gates for airborne weather radars with typical gate spacing of 75–150 m. Because a meteorological radar does not digitally sample the return signal at a sufficiently high rate, only a crude stepwise approximation to the surface echo is available. The peak of the narrow surface echo will be inaccurately determined in those instances where the surface echo is located, in range time, between two gates as a consequence of variation in aircraft altitude. In such situations, the magnitude of the surface echo can be negatively biased. The theoretical source of the error is discussed in section 2. Observations obtained by the National Aeronautics and

* Additional affiliation: Science Systems and Applications, Inc., Lanham, Maryland.

Corresponding author address: Dr. I. Jeff Caylor, NASA/GSFC, Code 912, Greenbelt, MD 20771.
E-mail: caylor@carmen.gsfc.nasa.gov

Space Administration (NASA) ER-2 Doppler radar (EDOP) are discussed in section 3. The EDOP radar operates at a wavelength of 3 cm and flies on the NASA ER-2 high-altitude aircraft. An algorithm is developed in section 4 that allows a correction to be applied to the surface echo on a sample by sample basis during post-processing. Conclusions are discussed in section 5.

2. Theoretical background

Radar altimeters and scatterometers operate with short pulse widths and sample the surface return at a high rate. In addition, such instruments are often designed to track the peak surface echo, all of which are aimed at providing a precise estimate of the surface echo. By comparison, weather radars are gated at fixed time increments referenced to the time of the transmitted pulse and the typical sample rate is proportional to the system bandwidth. Most meteorological radar receivers employ a passband filter with a width (B_6) matched to the length of the transmitted pulse ($B_6\tau = 1$), as an optimum compromise between range fidelity and signal-to-noise ratio (Zrnić and Doviak 1978). Doviak and Zrnić (1979) have shown that the range resolution volume for such a matched-filter receiver is nearly equal to the pulse width ($1.18c\tau/2$). As a consequence, the sampling interval, or gate spacing, on many weather radars is set to the pulse width. In fact, for meteorological targets it has been shown that sample intervals less than one-half the pulse width are of limited advantage (Urkowitz and Katz 1995). Unfortunately, scattering from the ocean surface imposes more stringent sampling requirements than for meteorological targets.

Microwave reflection from the ocean surface produces a relatively narrow impulse-like return. The amplitude of the surface echo at nadir incidence is a result of quasi-specular scattering and is modulated primarily by effects of the wind on the ocean surface, whereas the width of the surface echo is relatively insensitive to changes in the surface-wave characteristics for a 75-m gate spacing (Brown 1978; Elachi 1988). As will be shown for an idealized case, the shape of the surface echo is well approximated by a Gaussian function (Miller et al. 1991).

The surface echo can be modeled by the convolution of the surface impulse response, the specular point, and the point target response functions. Brown (1977) has developed a theoretical model for the microwave scattering from a rough surface such as the ocean. Brown gives the flat-surface impulse response $P(t)$ as

$$P(t) \approx C \exp\left(-\frac{4}{\gamma}\sin^2\xi - \frac{4ct}{\gamma h}\cos 2\xi\right) \times I_0\left[\frac{4}{\gamma}\left(\frac{ct}{h}\right)^{0.5}\sin 2\xi\right], \quad (1)$$

where t is time, h is aircraft altitude, ξ is the off-nadir antenna pointing angle, c the speed of light, and I_0 is a modified Bessel function of the second kind. The radar system parameters as well as the normalized surface cross section σ^o are incorporated in the constant C. Here $P(t)$ is the average power, as a function of time, scattered from a flat surface that has the same σ^o as the actual ocean surface. The antenna beamwidth parameter γ (Miller and Parsons 1985) is given by $\gamma = 2.885 \sin^2(\theta/2)$, with the half-power beamwidth denoted by θ.

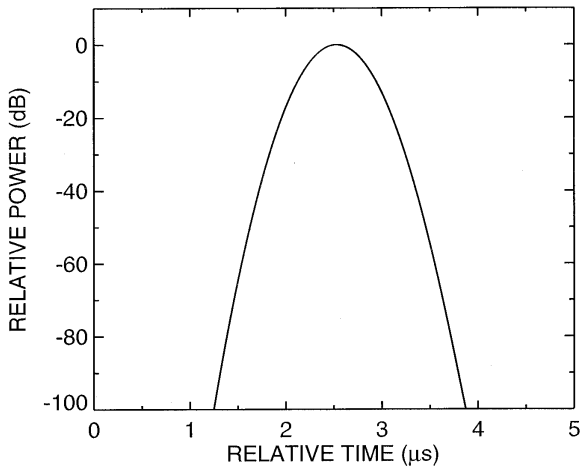

FIG. 1. Example of the received surface echo for nadir incidence ($\xi = 0$).

The received power waveform is found by convolving (1) with the receiver average power impulse response $Q(t)$. The receiver response is primarily dependent on the characteristics of the video filter, and for weather radar the response is typically well approximated by a Gaussian function (Doviak and Zrnić 1979; Miller and Parsons 1985; Kozu 1995). For a matched-filter receiver, the function

$$Q(t) = \exp\left(\frac{-\pi^2 t^2}{4\tau^2 \ln 2}\right) \quad (2)$$

is used for the normalized receiver average power impulse response (Doviak and Zrnić 1979). Using an altitude of 20 km and the EDOP system parameters (see section 3), the convolution of (1) and (2) was performed numerically. Figure 1 shows the results of a solution for the convolution at nadir incidence ($\xi = 0$).

A digital data acquisition system samples at discrete intervals, producing a stepwise approximation to the continuous return (Fig. 1). The peak surface echo will be increasingly well sampled as the distance between the peak and the nearest range gate diminishes. Digital sampling can be simulated by multiplying the received waveform with a comb function, that is, a series of delta functions separated by the range gate spacing (0.5 μs for EDOP). To demonstrate the effect of variable aircraft altitude, the continuous surface return is discretely sampled as the aircraft height is allowed to linearly increase, in effect shifting the surface echo to greater times rel-

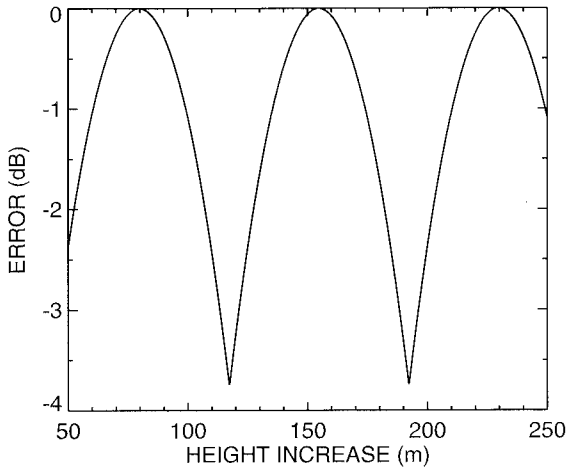

FIG. 2. The surface echo from Fig. 1 sampled with a gate spacing of 0.5 μs at nadir incidence. Aircraft altitude increases linearly.

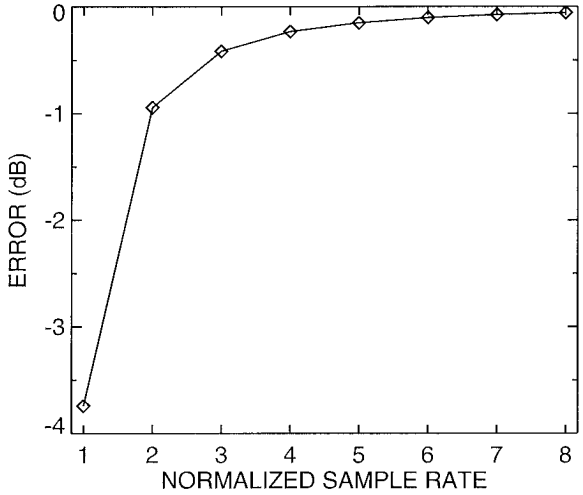

FIG. 3. Maximum error as a function of the normalized sample rate.

ative to the time of transmission. At each height increment, the range gate with the largest value is selected to represent the observed surface echo. Figure 2 shows the results of the demonstration; the sharp dips in the plot occur at points where the surface return is straddled by two range gates and the peak surface return is not accurately sampled. For the remainder of this paper, the *error* is defined as the deviation of the sampled return from the peak of the continuous return. The peak-to-peak variation in Fig. 2 directly corresponds to this error.

It is clear that the error will result in a negatively biased estimate of the peak surface echo and hence σ^o. The magnitude of the error is, though, related to the sampling frequency or range gate spacing. A higher sampling frequency will, other factors being equal, produce smaller errors. Using the EDOP system parameters, the error is investigated as a function of sample rate. The maximum error versus sample rate is shown in Fig. 3 for nadir incidence. The sample rate is normalized against the inverse of the pulse width; many conventional weather radars including EDOP employ a normalized sample rate of 1. The Nyquist sample rate that is twice the system bandwidth is given by a normalized rate of 2. Figure 3, which compares well with the results of Kozu et al. (1995), indicates that a significant reduction in the error to about 1 dB can be achieved by a doubling of the EDOP sample rate.

3. Example case

The observations described below were obtained with the EDOP X-band radar, which is housed in the nose of the NASA ER-2 aircraft that flies at a nominal altitude of 20 km and ground speed of 210 m s^{-1}. The EDOP radar operates at a frequency of 9.60 GHz and has an antenna beamwidth of 2.9°. The hardware is typically configured for a 0.5-μs pulse width and a 75-m range gate spacing. A more complete description of the radar system is provided by Heymsfield et al. (1996).

EDOP uses two antennas, one fixed at nadir and the other at approximately 33° forward of nadir. Because of the geometry for a large incidence angle, the forward surface echo is spread across a large number of range gates, and the resulting broad peak is sampled reliably. This is not the case for the nadir antenna. For ocean surface observations, the EDOP nadir signal is beam limited, which means that for the 2.9° beamwidth, the pulse width is long enough such that the surface lies completely within one resolution volume (Nathanson 1969). The result is that the surface echo rises above the receiver noise and peaks very rapidly, usually within one or two range gates. The exact shape of the surface echo itself is a complex function involving the antenna pattern, pulse shape, and response of the receiver in addition to the scattering characteristics of the surface itself (section 2).

As the aircraft changes altitude, the peak surface echo shifts from one gate to the next. It is during this transition between sampled range gates that the peak surface echo may be poorly estimated. Figure 4 shows an example, in a cloud-free region, of the normalized radar cross section σ^o where the aircraft is slowly increasing altitude. As the surface echo moves down range, the echo peak shifts from one range gate to the next (indicated by the dashed line). A minimum of 3–4 dB with respect to the maximum σ^o is observed, each time the peak echo moves between gates, at times 24, 103, 168, and 244 s. An additional minimum at 212 s is related to a small change in aircraft altitude, which did not result in a change of the surface gate. If an unbiased estimate of σ^o is represented by the value of the ''peaks'' in Fig. 4 where the surface echo is centered in the resolution volume, then the deviations to lower power will cause a negative bias in the estimate of the mean σ^o along

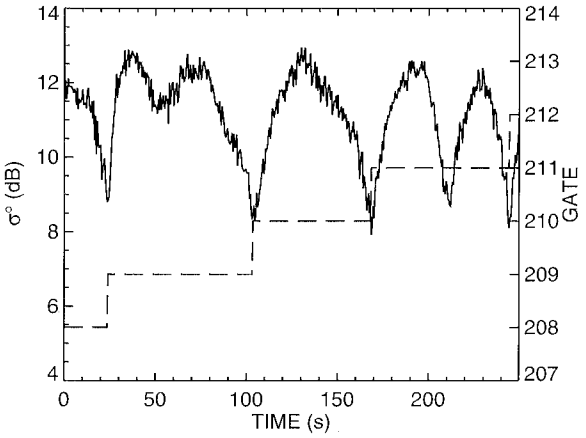

FIG. 4. Normalized surface cross section σ^o (solid line) observed at 2200 UTC 28 August 1995 at near-nadir incidence in a cloud-free region. The dashed line shows the range gate number where the surface peak echo is found. The dashed line indicates the increasing range to the surface as the aircraft changes altitude. The along-track distance is 52 km.

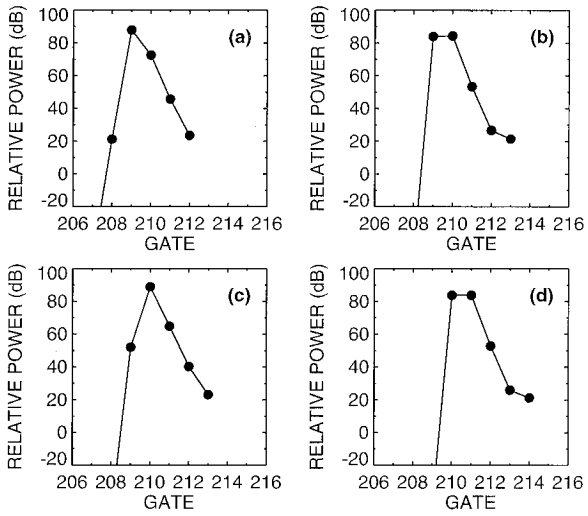

FIG. 5. Range profiles of the surface echo on 28 August 1995 at selected times from Fig. 4: (a) 70 s, (b) 103 s, (c) 130 s, and (d) 168 s. The gate spacing is 75 m.

the track. For the example in Fig. 4, the bias in the mean σ^o is approximately -1.5 dB. The exact value of the bias will depend on the length of the flight track and the rate of change in altitude of the aircraft. For the NASA ER-2, the aircraft is in slight ascent as a result of fuel burn-off so constant-altitude flight rarely occurs. In addition, aircraft altitude typically decreases during turns and altitude deviations also occur as a consequence of the disturbed atmosphere above large storms.

Example range profiles are shown in Fig. 5 for times 70, 103, 130, and 168 s from the flight track in Fig. 4. Figures 5a and 5c show the range profiles near maxima in Fig. 4, while profiles in the minima of Fig. 4 are shown in Figs. 5b and 5d. Clearly, the peak is not well sampled in Figs. 5b and 5d at times when the narrow surface echo is positioned between two gates. This loss of information for the echo peak results in the negative bias of the mean σ^o.

The surface echo rises very rapidly in one to two gates (75-m spacing) to reach the peak value, while there is a longer fall time for the 40–60-dB decrease on the down-range side of the peak. The asymmetry of the surface echo is attributed to several factors. The surface impulse response (1) contributes to the asymmetry near the peak of the echo as does a slower decay time, compared to the rise time, in the receiver's logarithmic amplifier (Skolnik 1990). The flat tail is possibly a result of antenna sidelobes.

4. Error correction algorithm

Several approaches to estimating the echo power from the surface with airborne radar have been suggested by Meneghini et al. (1989). The surface echo value can be simply the gate with largest power or an average of those gates that intersect the surface. Meneghini et al. also suggest fitting a quadratic to the three largest gates of the surface return in order to interpolate the maximum value. An attempt was made to interpolate the peak by applying both linear and nonlinear regression fits to the EDOP nadir profiles. This approach tended to produce inconsistent results for all types of profiles and when applied resulted in increased standard deviation for the mean σ^o along a flight track.

A second approach is to sum the received linear power at three range gates centered around the peak echo. It was found that using any more than three gates, the gate at the peak echo and one on either side, resulted in only negligible additional improvement because the surface echo falls off rapidly on both sides. Using additional gates in the sum can also create a positive bias in the σ^o estimate in areas of precipitation where the rain and mirror image echoes can become significant at gates removed from the surface. Tests have been performed with EDOP observations and typically approximately 2–3 dB can be recovered from points in the σ^o track where sampling errors occur. This will still leave residual 1-dB fluctuations in the σ^o data; a result in agreement with findings by Kozu et al. (1995).

A close examination of individual range profiles reveals that the gates near the surface peak undergo repetitive changes in relationship to each other as the surface echo moves between range gates. The relationship exists because the *shape* of the surface echo is relatively constant for the timescale of a normal flight track. The surface echo is well approximated by a Gaussian function (section 2), and the shape can be specified by the slope at specific points near the peak. Ratios between the peak gate and the gates on either side may be defined by

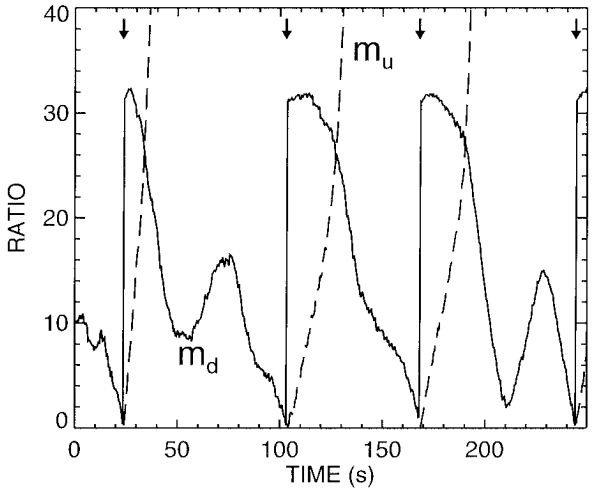

FIG. 6. Ratio of the signal in the gates around the peak surface echo for the data in Fig. 4. Ratio m_d is the solid line and m_u is the dashed line. The arrows indicate times at which the peak surface echo moved from one gate to the next.

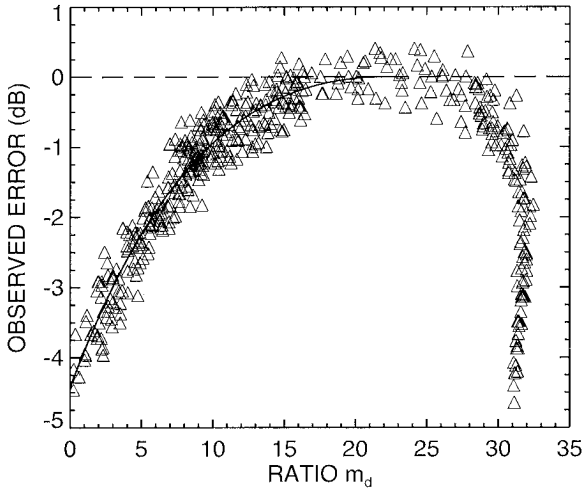

FIG. 7. Scatterplot of the ratio m_d versus estimated error from the baseline cross section for the data in Fig. 4. The solid line is the best-fit curve obtained from a regression analysis.

$$m_d = 10 \log\left[\frac{P(r_s)}{P(r_{s+1})}\right], \tag{3}$$

$$m_u = 10 \log\left[\frac{P(r_s)}{P(r_{s-1})}\right], \tag{4}$$

where P is the received power. The range to the ith gate is r_i with r_s indicating the gate containing the peak surface echo. Ratios m_d and m_u are proportional to the slope on the down-range and up-range sides of the surface echo peak in logarithmic terms. Defining the ratios by (3) and (4) allows the correction algorithm to function regardless of whether the power, reflectivity Z, or cross section σ^o is used. Only three gates, the peak and gates on either side, are considered because at greater ranges from the surface the return will be increasingly affected by antenna sidelobes and meteorological backscatter.

Values of m_u and m_d for the 28 August 1995 example case are shown in Fig. 6. At points where the surface echo peak moves between gates, both ratios are near zero indicating an inadequately sampled range profile with a flattened peak (e.g., Figs. 5b and 5d). The breaks in the m_u curve (dashed line) are caused by $P(r_{s-1})$ dropping below the receiver noise threshold, while the steep slope is because the leading edge of the surface echo rises out of the noise very rapidly. Note that m_d does not exhibit similar behavior because the down-range side of the surface echo does not fall off as rapidly (see Fig. 5). The ratios exhibit repetitive characteristics each time the peak moves through a gate. A method to use (3) and (4) for correction of the error in the cross-sectional estimate therefore requires only establishing a relationship between specific values of the ratios and the observed error. A scatterplot that emphasizes the relationship between the offset from the peak σ^o and m_d is shown in Fig. 7 for the 2200 UTC example.

The zero-level baseline σ^o can be identified by regions where m_d is high (i.e., when the peak is centered near a gate), and so the error in Fig. 7 is chosen relative to σ^o where $15 < m_d < 25$. It is clear from Fig. 7 that there is a well-behaved relationship between m_d and the error. The random scatter of approximately ± 0.5 dB is seen as the small, higher frequency deviations in Fig. 4. An obvious problem for a potential correction algorithm is that for $m_d > 30$, the slope in Fig. 7 becomes very large. This would translate into large changes in the correction factor as a result of small errors in the computed m_d. Therefore, for a m_d above about 25, the m_u ratio (4) is instead used to compute the correction. The exact point to switch from m_d to m_u is determined by simply selecting the larger of the gates on either side of the peak,

$$m = \begin{cases} m_u, & P(r_{s-1}) > P(r_{s+1}) \\ m_d, & P(r_{s-1}) \le P(r_{s+1}). \end{cases} \tag{5}$$

The m_u observations are shown in Fig. 8 for points where $m_u > m_d$.

A regression was performed on the data in Figs. 7 and 8 to determine the coefficients for a pair of fourth degree polynomials. The baseline is further refined (usually less than 0.25 dB) by requiring the peak of the fitted curve to have an offset of zero; that is, large ratios have zero offset. The error correction for each beam is achieved by first computing ratios m_d and m_u from three gates associated with the surface return. The regression polynomials are then used to determine the correction to apply to the observed σ^o at that time. The curves from the regression analysis, shown in Figs. 7 and 8, typically have an rms error of about 0.3 dB. Figure 9 shows the results of the bias correction using the ratio

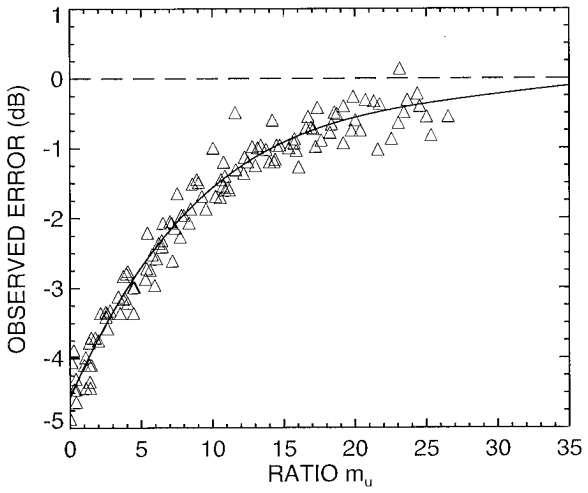

FIG. 8. As in Fig. 7 except for ratio m_u versus estimated error. The data are plotted only for points where $P(r_{s-1}) > P(r_{s+1})$.

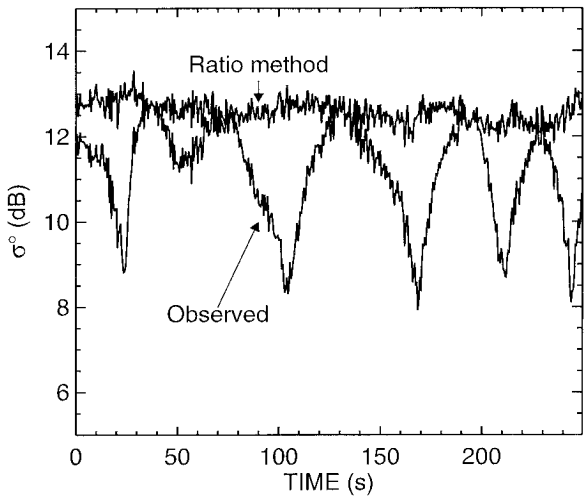

FIG. 9. Ocean cross section as in Fig. 4, with an error correction derived from the ratio data shown in Figs. 7 and 8.

method for the 2200 UTC case. The mean of the logarithmic samples is 11.2 ± 1.2 dB for the observed data, while the ratio method results in $\sigma^o = 12.6 \pm 0.3$ dB and performs slightly better than the three-gate sum, which gives $\sigma^o = 11.9 \pm 0.5$ dB. The corrected σ^o value of 12.6 dB is consistent with observations at nadir incidence by Masuko et al. (1986).

As a second example, a 124-km flight track at 2203 UTC 28 August 1995 was selected for a thunderstorm with significant path attenuation caused by heavy rain ($Z_e > 50$ dBZ). Figure 10a shows the observed σ^o that exhibits a number of deviations along the track. The polynomials computed from the example data (Fig. 4) were used to correct σ^o and the result is shown in Fig. 10b. With the exception of excursions between 260 and 470 s, all others were removed. The low values of σ^o do not represent absolute surface cross section but are indications of attenuation along the propagation path caused by heavy precipitation. The dashed line in Fig. 10b shows the two-way path-integrated attenuation as estimated from a k–Z relationship ($k = 2.9 \times 10^{-4} Z^{0.72}$; Battan 1973), which indicates a high correlation with the corrected σ^o. The estimated attenuation is smaller than the attenuation derived from σ^o because the k–Z calculation was performed on the observed reflectivity profiles that are already influenced by attenuation.

A caveat to the ratio algorithm as described above is that the relationship of the values at gates around the surface echo peak changes as a function of incidence angle. As a result, a given pair of polynomials will be valid only for a small range of incidence angles. It has been determined from the EDOP data that the polynomials derived for near-nadir observations become inaccurate when the incidence angle exceeds approximately 3° (a beamwidth). In level flight this is not a severe problem, but a family of polynomials can be developed for off-nadir angles in a similar manner as described above. Figure 11 shows the theoretical error as a function of off-nadir angle for the EDOP current configuration of 0.5-μs gate spacing. There is about 3-dB variation in the error over 10°, although by doubling the sample rate not only would the maximum error be reduced to 0.9 dB but the variation as a function of incidence angle is also less significant at only about 0.8 dB.

Also shown on Fig. 11 by the dashed line, is the error for a satellite-borne radar. The parameters used for the calculations are for a matched-filter receiver with system characteristics similar to those of the precipitation radar to be flown on the NASA Tropical Rainfall Measuring Mission (Simpson et al. 1988). This radar performs

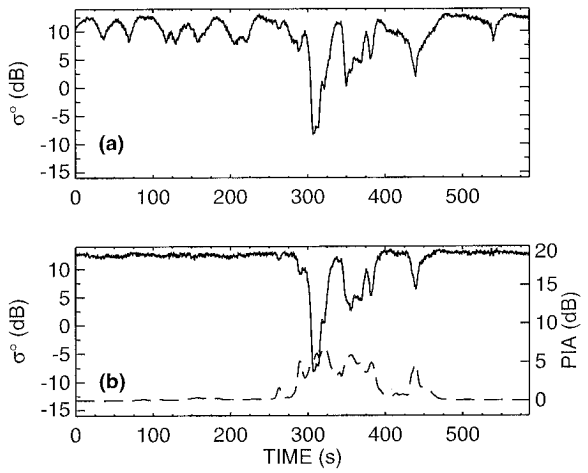

FIG. 10. (a) Observed surface cross section under a storm at 2203 UTC 28 August 1995. The along-track distance is 124 km. (b) The σ^o corrected using the ratio method described in the text. The remaining deviations (260–470 s) are a result of attenuation by rain along the propagation path. An estimate of the path-integrated attenuation (PIA) from the observed precipitation reflectivity factor is shown by the dashed line.

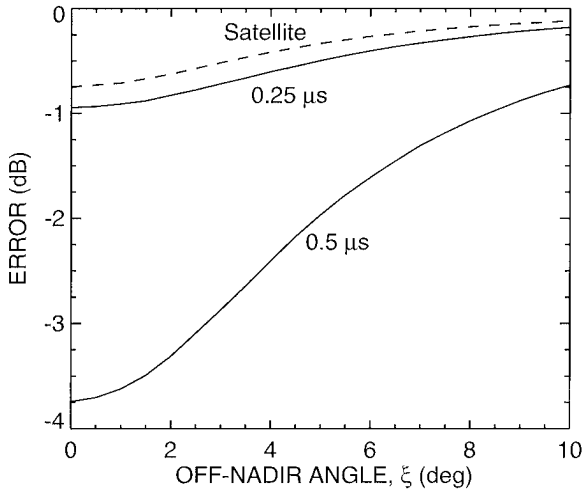

FIG. 11. Computed error as a function of the antenna angle off-nadir (ξ) using the EDOP system parameters. Errors are shown for gate spacings of 0.5 μs (current configuration) and 0.25 μs. The dashed line is for a radar such as will be flown on the NASA TRMM satellite.

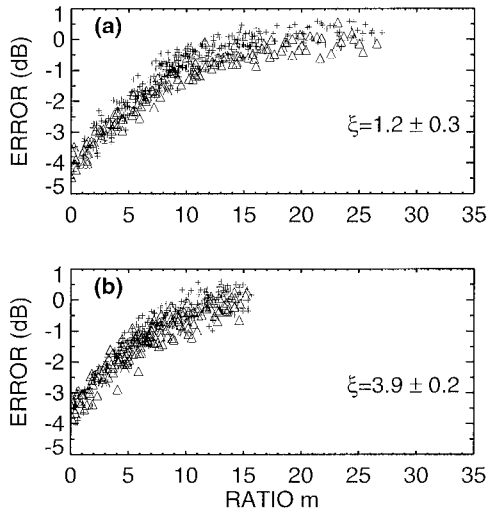

FIG. 12. (a) Scatterplot of m versus estimated error for the data shown in Fig. 4. The mean incidence angle is 1.2°. (b) Example of m for a case at 1757 UTC 11 January 1995, where the mean incidence angle is 3.9°. In both panels, the contributions are shown for m_d (+) and m_u (△).

cross-track scanning, and because the 0.71° beamwidth is relatively narrow compared to the incidence angle, the surface impulse response function (1) was modified with the approximation described by Brown (1989) for $\xi \geq 5°$. The receiver impulse response that was used is that given by Kozu (1995). In anticipation of the type of problems described in this paper, the TRMM radar will perform oversampling with gate spacing of half a pulse width, and as a result the error is expected to be less than 0.75 dB for all scan angles.

A scatterplot of m versus offset is shown in Fig. 12a for the 2200 UTC 28 August 1995 case where the mean incidence angle is 1.2°. At a higher incidence angle of 3.9° (Fig. 12b, 1757 UTC 11 January 1995), the curve is similar in shape but truncated at $m = 15$, which indicates the surface echo has been broadened. As the incidence angle increases, the surface return is broadened, and m_d and m_u will have a smaller dynamic range, with values approaching zero. Near $m = 0$, there is an approximately 0.75-dB difference between the data for the two angles, which agrees reasonably well with the 1 dB estimated from Fig. 11.

Since (5) is a combination of (3) and (4), the contributions to ratio m from m_d (+ symbols) and m_u (△ symbols) are differentiated in Fig. 12. The m_u contributions typically have a slightly larger ratio, that is, steeper rise, for the same offset because of the asymmetry in the surface echo as a result of the antenna sidelobes (see Fig. 5). This feature can be seen in Fig. 12a, and other EDOP observations show it more clearly. A regression fit to the m data, therefore, does not perform quite as well as the two-ratio algorithm described above since it would not distinguish between down- and up-range sides of the surface echo.

5. Conclusions

Deviations of 3–4 dB in the return from the ocean surface have been observed with the EDOP airborne radar at nadir incidence. These deviations are correlated with changes in aircraft altitude and arise from the fixed gating (range sampling) normally used in a weather radar, which, at times, makes it difficult to estimate the peak value of the narrow surface echo. A number of airborne radar analysis techniques require estimates of the surface cross section; in particular, the surface reference methods for estimating path-integrated attenuation through precipitation and the observed deviations of 3–4 dB can be as large as those occurring from attenuation in precipitation. A correction, therefore, needs to be applied to the surface cross section for observations at near-nadir incidence angles.

The values of the range gates on each side of the peak return are shown to exhibit a relationship to the peak as the surface echo moves between two gates. The functional relation between the gates is a result of the surface scattering physics and the radar system characteristics such as antenna pattern, pulse shape and width, and receiver response. This empirical relationship forms the basis of a simple statistical algorithm that can be used to correct the bias in the mean surface cross section for observations in both cloud-free and rainy regions. Because wave height and surface roughness can change significantly from day to day, the most reliable results have been obtained by computing correction polynomials for each flight line. All that is required to develop a similar relationship for any particular airborne weather radar is a slowly ascending or descending flight track over cloud-free ocean.

The findings of this paper are of concern to existing

airborne radar and future spaceborne weather radar. The EDOP radar employs a matched-filter receiver currently and samples in range at a rate that is equal to the receiver bandwidth. As shown in Fig. 3, errors of 4 dB can be reduced to approximately 1 dB by doubling the sample rate. Further reductions can be achieved by higher sample rates but at the cost of increasing the computational and storage requirements of the data acquisition system. Observations of σ^o as a function of wind speed (Barrick 1974; Brown 1979) suggest that the natural variability is such that reduction of the error below about 0.5–0.75 dB is of negligible benefit. The issue of oversampling will be investigated with observations from future flights of the EDOP radar as well as with data from other airborne radars.

Acknowledgments. The authors wish to thank the EDOP instrument engineer, Dr. Steve Bidwell, for his outstanding efforts. This research is funded under NASA RTOP 460-24-52.

REFERENCES

Atlas, D., and T. J. Matejka, 1985: Airborne Doppler radar velocity measurements of precipitation seen in ocean surface reflection. *J. Geophys. Res.,* **90** (D3), 5820–5828.

Barrick, D. E., 1974: Wind dependence of quasispecular microwave sea scatter. *IEEE Trans. Antennas Propag.,* **AP-22,** 135–136.

Battan, L. J., 1973: *Radar Observation of the Atmosphere.* University of Chicago Press, 324 pp.

Brown, G. S., 1977: The average impulse response of a rough surface and its applications. *IEEE Trans. Antennas Propag.,* **AP-25,** 67–74.

——, 1978: Backscattering from a Gaussian-distributed perfectly conducting rough surface. *IEEE Trans. Antennas Propag.,* **AP-26,** 472–482.

——, 1979: Estimation of surface wind speeds using satellite-borne radar measurements at normal incidence. *J. Geophys. Res.,* **84,** 3974–3978.

——, 1989: A useful approximation for the flat surface impulse response. *IEEE Trans. Antennas Propag.,* **37,** 764–767.

Doviak, R. J., and D. Zrnić, 1979: Receiver bandwidth effect on reflectivity and Doppler velocity estimates. *J. Appl. Meteor.,* **18,** 69–76.

Durden, S. L., E. Im, F. K. Li, W. Ricketts, A. Tanner, and W. Wilson, 1994: ARMAR: An airborne rain-mapping radar. *J. Atmos. Oceanic Technol.,* **11,** 727–737.

Elachi, C., 1988: *Spaceborne Radar Remote Sensing: Applications and Techniques.* IEEE Press, 255 pp.

Heymsfield, G. M., and Coauthors, 1996: The EDOP radar system on the high-altitude NASA ER-2 aircraft. *J. Atmos. Oceanic Technol.,* **13,** 795–809.

Hildebrand, P. H., 1994: Estimation of sea-surface winds using backscatter cross-section measurements from airborne research weather radar. *IEEE Trans. Geosci. Remote Sens.,* **32,** 110–117.

Iguchi, T., and R. Meneghini, 1994: Intercomparison of single-frequency methods for retrieving a vertical rain profile from airborne or spaceborne radar data. *J. Atmos. Oceanic Technol.,* **11,** 1507–1516.

Kozu, T., 1995: A generalized surface echo radar equation for down-looking pencil beam radar. *IEICE Trans. Commun.,* **E78-B,** 1245–1248.

——, T. Manabe, Y. Katoh, and S. Terushita, 1995: Earth surface remote sensing with TRMM radar. *Tech. Rep. of the Institute of Electronics, Information and Communication Engineers,* **SANE94-95(1995-02),** 17–22.

Masuko, H., K. Okamoto, M. Shimada, and S. Niwa, 1986: Measurement of microwave backscattering signatures of the ocean surface using X band and K_a band airborne scatterometers. *J. Geophys. Res.,* **91,** 13 065–13 083.

Meneghini, R., and K. Nakamura, 1990: Range profiling of the rain rate by an airborne weather radar. *Remote Sens. Environ.,* **31,** 193–209.

——, J. Eckerman, and D. Atlas, 1983: Determination of rain rate from a spaceborne radar using measurements of total attenuation. *IEEE Trans. Geosci. Remote Sens.,* **GE-21,** 34–43.

——, K. Nakamura, C. W. Ulbrich, and D. Atlas, 1989: Experimental tests of methods for the measurement of rainfall rate using an airborne dual-wavelength radar. *J. Atmos. Oceanic Technol.,* **6,** 637–651.

Miller, L. S., and C. L. Parsons, 1985: The effect of microwave backscatter uncertainty on satellite radar altimetry accuracy. *IEEE J. Oceanic Eng.,* **OE-10,** 438–442.

——, G. S. Brown, and L. W. Choy, 1991: Multibeam radar altimetry: Spaceborne feasibility. *IEEE Trans. Geosci. Remote Sens.,* **29,** 465–469.

Nathanson, F. E., 1969: *Radar Design Principles.* McGraw-Hill, 626 pp.

Simpson, J., R. F. Adler, and G. North, 1988: A proposed tropical rainfall measuring mission (TRMM) satellite. *Bull. Amer. Meteor. Soc.,* **69,** 278–295.

Skolnik, M. I., Ed., 1990: *Radar Handbook.* 2d ed. McGraw-Hill.

Urkowitz, H., and S. L. Katz, 1995: The relation between range sampling rate, system bandwidth, and variance reduction in spectral averaging for meteorological radar. Preprints, *27th Conf. Radar Meteorology,* Vail, CO, Amer. Meteor. Soc., 756–758.

Zrnić, D., and R. J. Doviak, 1978: Matched filter criteria and range weighting for weather radar. *IEEE Trans. Aerosp. Electron. Syst.,* **14,** 925–930.